SISSA

Hunting dark matter gamma-ray lines with the Fermi LAT

To cite this article: Gilles Vertongen and Christoph Weniger JCAP05(2011)027

View the article online for updates and enhancements.

Hunting dark matter gamma-ray lines with the Fermi LAT

Gilles Vertongen[a] and Christoph Weniger[b]

[a]Deutsches Elektronen-Synchrotron (DESY),
Notkestrasse 85, 22603 Hamburg, Germany

[b]Max-Planck-Institut für Physik,
Föhringer Ring 6, 80805 München, Germany

E-mail: gilles.vertongen@desy.de, weniger@mppmu.mpg.de

Abstract. Monochromatic photons could be produced in the annihilation or decay of dark matter particles. At high energies, the search for such line features in the cosmic gamma-ray spectrum is essentially background free because plausible astrophysical processes are not expected to produce such a signal. The observation of a gamma-ray line would hence be a 'smoking-gun' signature for dark matter, making the search for such signals particularly attractive. Among the different dark matter models predicting gamma-ray lines, the local supersymmetric extension of the standard model with small R-parity violation and gravitino LSP is of particular interest because it provides a framework where primordial nucleosynthesis, gravitino dark matter and thermal leptogenesis are naturally consistent. Using the two-years Fermi LAT data, we present a dedicated search for gamma-ray lines coming from dark matter annihilation or decay in the Galactic halo. Taking into account the full detector response, and using a binned profile likelihood method, we search for significant line features in the energy spectrum of the diffuse flux observed in different regions of the sky. No evidence for a line signal at the 5σ level is found for photon energies between 1 and 300 GeV, and conservative bounds on dark matter decay rates and annihilation cross sections are presented. Implications for gravitino dark matter in presence of small R-parity violation are discussed, as well as the impact of our results on the prospect for seeing long-lived neutralinos or staus at the LHC.

Contents

1 Introduction

Gravitational evidences for dark matter exist from galactic to cosmological scales, but its particle nature still remains unknown [1–3]. The most popular dark matter candidate, a weakly interacting massive particle (WIMP), could in principle be detected directly through its scattering on atomic nuclei, indirectly by observing traces of its annihilation products in the cosmic-ray fluxes, or by its direct production at colliders. Since the stability of dark matter is by no means established, there is also the possibility to observe cosmic-ray contributions stemming from its decay. However, despite lots of efforts, no unambiguous non-gravitational dark matter signal has been found so far.

Indirect searches for dark matter annihilation or decay products in the cosmic gamma-ray, anti-particle and neutrino fluxes are limited not only by the instrument sensitivities, but also by our understanding of the astrophysical foregrounds. One of the few dark matter signatures that would unambiguously stand out of the astrophysical foreground are the monochromatic photons potentially produced in two-body annihilation or decay of dark matter. They would appear as a line feature in the otherwise continuous gamma-ray energy spectrum [1–6]. The observation of such a gamma-ray line would thus be of paramount interest for the understanding of dark matter in the Universe.

The production of gamma-ray lines is expected in many theoretical dark matter models. The corresponding branching ratios are often very small, but this could be compensated by the high experimental sensitivity to such signals. In the popular scenario where dark matter is the lightest neutralino χ_1^0 of the minimal supersymmetric standard model (MSSM) [7], gamma-ray lines from $\chi_1^0\chi_1^0 \to \gamma\gamma$ or $\chi_1^0\chi_1^0 \to \gamma Z^0$ annihilations are only produced at the one-loop level [8–14], and they would be mostly out of reach for current experiments. However, their production can be enhanced in non-minimal variations of the MSSM [15, 16]. Alternatively, a large number of viable WIMP models exist, some of them predicting a sizable annihilation into monochromatic photons, e.g. singlet dark matter [17], hidden U(1) dark matter [18–20], effective dark matter scenarios [21], scenarios with strong annihilation into the higgs boson and a photon [22], inert higgs doublet dark matter [23], or Kaluza-Klein

dark matter in models with universal extra dimensions [24, 25]. Additionally, prominent spectral features in the gamma-ray flux can be generated by the internal Bremsstrahlung or final state radiation potentially produced in dark matter annihilation [26–29].

An interesting example of decaying dark matter is the gravitino $\psi_{3/2}$, which appears in locally supersymmetric extensions of the Standard Model. In scenarios where R-parity and the lepton number are slightly violated and the gravitino is the lightest superparticle (LSP), thermal leptogenesis, gravitino dark matter and primordial nucleosynthesis are naturally consistent [30]. Within this framework, the gravitino is no longer stable and decays on cosmological time scales [31], thus rendering the imprints of its decay potentially observable in the cosmic-ray fluxes [32–43]. Interestingly, the line feature generated by the two-body decay into neutrinos and photons, $\psi_{3/2} \to \gamma\nu$, is prominent for a wide range of gravitino masses [33], suggesting that the first observation of gravitino dark matter could happen via gamma-ray lines.

In general, dark matter lifetimes of the order of 10^{26}–10^{29} s, which is in the ballpark of what is accessible by cosmic-ray experiments in the GeV–TeV regime, are obtained when the symmetry responsible for the dark matter stability is violated by dimension six operators generated close to the grand unification scale [44, 45]. A typical example, which has a large branching fraction into monochromatic photons, is the hidden SU(2) vector dark matter [46]. Note that even if dark matter only decays into charged leptons at tree level, like in the models designed to explain the PAMELA/Fermi LAT $e^{\pm}$ measurements [47–49], gamma-ray lines produced at the one-loop level could potentially be observable [50].

A dedicated search for Galactic gamma-ray lines with energies between 30 and 200 GeV using the Fermi Large Area Telescope (LAT) data [51] has been presented in ref. [52], where the all-sky averaged diffuse gamma-ray flux measured between 7 Aug 2008 and 21 Jul 2009 was considered. Searching for monochromatic features in the energy spectrum, their null result enable them to put constraints on the dark matter annihilation cross section and decay rate into gamma-ray lines. A similar analysis using the EGRET[1] data has been performed for gamma-ray line energies between 0.1 and 10 GeV in ref. [53].

The extra-galactic gamma-ray background (EGBG), as derived from the Fermi LAT data in ref. [54], has also been used in ref. [55] to put constraints on gamma-ray lines from cosmological dark matter annihilation [56, 57]. In that case, the redshifted gamma-ray lines lead to less pronounced features in the energy spectrum than the Galactic ones. The lack of spectral features in the EGBG was used to put limits on the corresponding annihilation cross section. Further gamma-line searches, coming from different observations, and ranging from energies of 10 keV up to 10 TeV, were presented for annihilation in ref. [58] and for decay in ref. [59]. General strategies for the detection of gamma-ray lines from dark matter annihilation with Fermi LAT and future experiments were discussed in refs. [60–62].

The purpose of this paper two-fold: first, we will update and extend the gamma-ray line analysis of the Fermi LAT data presented in ref. [52] to a larger energy range of 1–300 GeV, searching for significant line signals that might come from dark matter annihilating or decaying in the Galactic dark matter halo, and derive conservative constraints. Although highly relevant for the gravitino dark matter scenario, no dedicated search for gamma-ray lines from decaying dark matter in the whole $\mathcal{O}(\text{GeV–TeV})$ energy regime has been performed so far. Furthermore, the large statistics of the Fermi LAT data allows us to further probe the low energy regime, i.e. energies from 1 to 10 GeV, and thus strengthening the previous

---

[1]See http://heasarc.gsfc.nasa.gov/docs/cgro/cgro/egret.html.

EGRET bounds on annihilating dark matter [53]. Such energies are of particular interest in the view of the recent hints from direct dark matter detection reported by the CDMS [63], CoGeNT [64] and DAMA [65, 66] collaborations. Second, we will discuss the impact of our results on decaying gravitino dark matter. Covering previously unexplored values of the gravitino mass, we will use our limits on gamma-ray lines to constrain the size of R-parity violation, which can be translated into lower limits on the decay lengths of neutralino or stau NLSPs.

The paper is organized as follows: in section 2, we present our analysis of the Fermi LAT data. After briefly discussing the gamma-ray flux produced in the dark matter annihilation or decay, we present the strategy for data extraction and line searches in section 2.1. Section 2.2 is devoted to a presentation of the resulting bounds on annihilation cross section and decay rate, whereas in section 2.3 we discuss details and caveats of our analysis. In section 3, we apply our results to gravitino dark matter and discuss prospects for NLSP observations at particle colliders. We then conclude in section 4.

2 Gamma-ray line constraints from Fermi LAT

Our line search is based on the measurements of the cosmic gamma-ray flux performed since August 2008 by the Large Area Telescope (LAT), the main instrument on the Fermi Gamma-ray Space Telescope. The LAT is a pair conversion detector, designed to observe gamma rays with energies ranging from 30 MeV to more than 300 GeV with an energy resolution of about 10%. It has a large field-of-view that spans around 20% of the sky, allowing an effective measurement of the all-sky diffuse fluxes. From the four event classes presented in the available public data, we only consider the recently released 'DataClean' event class, which provides the best rejection of charged cosmic rays. This is especially important when analyzing the diffuse gamma-ray flux at high energies.

Gamma-ray lines may find their origin in the decay or annihilation of dark matter particles ψ in the Galactic halo. The observed gamma-ray flux at Earth is given by a line-of-sight integral depending linearly on the dark matter distribution $\rho_{\rm dm}(r)$ when considering dark matter decays

$$\frac{dJ_\gamma}{dE}(\xi) = \frac{\Gamma_{\psi\to\gamma\nu}}{4\pi\,m_\psi}\,\delta\!\left(E - \frac{m_\psi}{2}\right)\underbrace{\int_{\rm l.o.s.} ds\,\rho_{\rm dm}(r)}_{\equiv J_\rho^{\rm dec.}},\tag{2.1}$$

while in the annihilation case, it depends quadratically on $\rho_{\rm dm}(r)$

$$\frac{dJ_\gamma}{dE}(\xi) = 2\,\frac{\langle\sigma v\rangle_{\psi\psi\to\gamma\gamma}}{8\pi\,m_\psi^2}\,\delta(E - m_\psi)\underbrace{\int_{\rm l.o.s.} ds\,\rho_{\rm dm}^2(r)}_{\equiv J_\rho^{\rm ann.}}\,.\tag{2.2}$$

Here, m_ψ is the dark matter mass, while $\Gamma_{\psi\to\gamma\nu}$ and $\langle\sigma v\rangle_{\psi\psi\to\gamma\gamma}$ denote the dark matter decay width and annihilation cross section into gamma-ray lines, respectively. The coordinate s runs along the line of sight, in a direction spanning an angle ξ with respect to the Galactic center direction. The distance to the Galactic center r is related to the distance to the Sun s through $r(s,\xi) = \sqrt{(r_0 - s\cos\xi)^2 + (s\sin\xi)^2}$, where $r_0 = 8.5\,{\rm kpc}$ is the distance of the Sun to the Galactic center [67, 68].

Target region	Geometry	$\int_{\Delta\Omega} d\Omega\, J_\rho^{\mathrm{dec.}}$	$\int_{\Delta\Omega} d\Omega\, J_\rho^{\mathrm{ann.}}$
		[GeV cm^{-2} sr]	[GeV^2 cm^{-5} sr]
Halo	$|b| \geq 10°$	2.2×10^{23}	8.3×10^{22}
Center	$|l| \leq 36°$ and $5° \leq |b| \leq 36°$ *plus* $|l| \leq 7°$ and $|b| \leq 5°$	6.9×10^{22}	9.2×10^{22}

Table 1. Geometry of our target regions in terms of Galactic longitude l and latitude b. The line-of-sight integrals $J_\rho^{\mathrm{dec.}}$ and $J_\rho^{\mathrm{ann.}}$ integrated over the target regions are also shown, assuming a NFW profile.

We consider the Navarro-Frenk-White (NFW) profile [52, 69]

$$\rho_{\mathrm{dm}}(r) = \rho_0 \left[\frac{r}{r_0}\right]^{-\gamma} \left[\frac{1 + (r_0/r_s)^\alpha}{1 + (r/r_s)^\alpha}\right]^{\frac{\beta-\gamma}{\alpha}}, \tag{2.3}$$

which is defined by $(\alpha, \beta, \gamma) = (1, 3, 1)$ and $r_s = 20\,\mathrm{kpc}$, as a reference for the dark matter distribution. For the sake of comparison, we also consider the isothermal profile with $(\alpha, \beta, \gamma) = (2, 2, 0)$ and $r_s = 3.5\,\mathrm{kpc}$, as well as the Einasto profile [70–72]

$$\rho_{\mathrm{dm}}(r) = \rho_0 \exp\left[-\frac{2}{\alpha}\left(\frac{r^\alpha - r_0^\alpha}{r_s^\alpha}\right)\right] \quad \text{with} \quad \alpha = 0.17, \quad r_s = 20\,\mathrm{kpc}, \tag{2.4}$$

which is favored by the latest N-body simulations.[2] All profiles are normalized to $\rho_0 = 0.4\,\mathrm{GeV}\,\mathrm{cm}^{-3}$ at Sun's position [74, 75]. The resulting line-of-sight integrals $J_\rho^{\mathrm{dec.}}$ and $J_\rho^{\mathrm{ann.}}$, integrated over our target regions (see below), are summarized in table 1 for the NFW profile. Note that substructures in the Galactic dark matter distribution can change the angular profile and magnitude of the gamma-ray emission (see e.g. refs. [62, 72]). If this is the case, our results can straightforwardly be generalized by adopting the corresponding values for $J_\rho^{\mathrm{dec./ann.}}$.

2.1 Methods

The gamma-ray events that enter our analysis are selected from the 'DataClean' event class of the Fermi LAT data measured between 4 Aug 2008 and 17 Nov 2010.[3] From all events recorded by the Fermi LAT, we select energies between 100 MeV and 500 GeV, and apply the zenith angle criterion $\theta < 105°$ in order to avoid contamination by the Earth's Albedo.[4] Below 1 GeV, the fast variation of the effective area as well as the presence of small and sharp jumps in the energy spectrum (presumably related to side effects of the energy reconstruction [76, 77]) introduce spurious effects in our line search. Furthermore, the nominal energy range of the Fermi LAT ends at 300 GeV [51]. As a consequence, we concentrate on gamma-ray line energies between 1 and 300 GeV. Systematic uncertainties, as well as limitations of the analysis method, are discussed in section 2.3 in light of the data.

---

[2]However, see ref. [73] for observational arguments in favor of cored dark matter profiles.

[3]The event data, as well as the corresponding information about the instrument response functions concerning angular and energy resolution, are available at `http://fermi.gsfc.nasa.gov/ssc/data/`.

[4]These selections are made using the Fermi Science Tools v9r18p6, see `http://fermi.gsfc.nasa.gov/ssc/data/analysis/software/`. As cut in `gtmktime` we took `DATA_QUAL==1 && LAT_CONFIG==1 && ABS(ROCK_ANGLE)<52`.
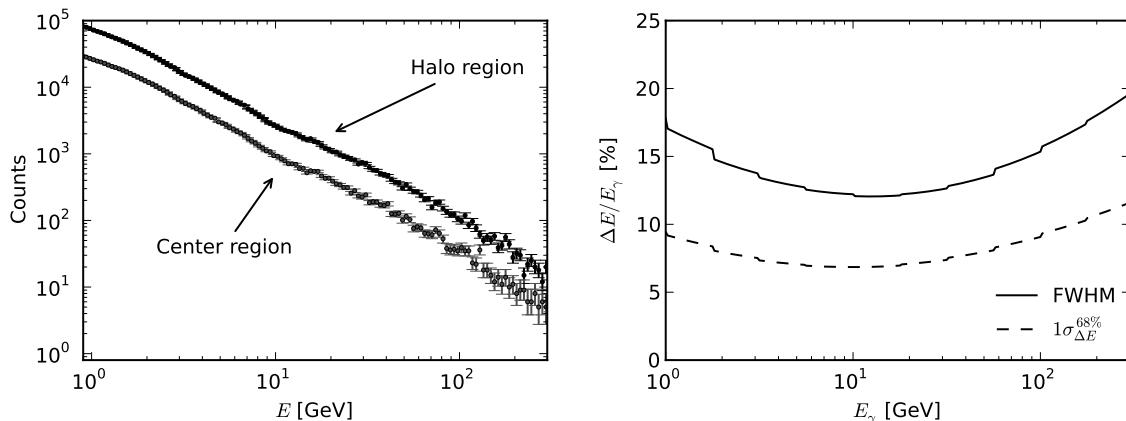
Figure 1. *Left panel*: observed counts in the halo and the center regions, binned into 50 bins per energy decade (200 bins per decade are used in our likelihood analysis). *Right panel*: Fermi LAT energy resolution $\Delta E/E_\gamma$, in terms of FWHM and 68% containment $\sigma_{\Delta E}^{68\%}$, as derived from the IRF of the 'DataClean' event class.

When looking for dark matter signals in gamma-ray maps that cover the whole sky, it is critical to choose a target region which maximizes the corresponding signal-to-noise ratio S/N. The two regions that we found giving a very good S/N for decaying dark matter ('halo region') or annihilating dark matter ('center region') are summarized in table 1. Although optimized for the NFW profile, they also yield good S/N for the Einasto and isothermal profiles.

Since the selection procedure leaves us with a large number of 1.3×10^6 (5×10^5) events above $1 \, \mathrm{GeV}$ for the halo (center) region, we perform a binned analysis of the data. To this end, we distribute the events into 200 logarithmically equally spaced energy bins per decade, and sum over the angles. This gives a sequence of count numbers $c_i \in \mathbb{N}_0$, which is illustrated in the left panel of figure 1 for both target regions. Note that we do not perform a point source subtraction in this work. A proper treatment would mask out only $\mathcal{O}(5\%)$ of the events [52], and hence only marginally affect our results.

The spectral feature produced by a gamma-ray line can be inferred from the Fermi LAT instrument response function (IRF). Its most recent version, 'Pass6 version 3', was determined using Monte Carlo generated samples of photon events between $18 \, \mathrm{MeV}$ and $562 \, \mathrm{GeV}$, and includes effects measured in-flight, see refs. [78, 79]. It contains the point-spread-function (PSF), as well as the energy dispersion $\mathcal{D}(E, E_\gamma)$ which describes the distribution of the reconstructed energies E as a function of the physical photon energy E_γ. In order to integrate out the implicit dependence of the energy dispersion on the event impact angle with respect to the detector axis, $\mathcal{D}(E, E_\gamma)$ is averaged over this impact angle weighted by its distribution in our data sample. The resulting full width at half maximum (FWHM) of the energy dispersion is shown in the right panel of figure 1, where the 68% containment energy resolution $\sigma_{\Delta E}^{68\%}$ is also shown.[5] Lastly, since our two samples have a large sky coverage, the effects of the PSF, which features a 68%-containment angle well below 1° at energies above $1 \, \mathrm{GeV}$, can safely be neglected.

---

[5]Our resulting FWHM is larger than the one discussed in ref. [52] by a factor of 1.1–1.4, which presumably affects our limits at the level of 5%–20%. The difference is probably due to different energy reconstruction methods underlying the public 'DataClean' event class used in this work and the dedicated analysis in ref. [52]. However, the 68% containment agrees well with ref. [51].

The profile likelihood method [80, 81] is used to calculate the significance of a potential gamma-ray line contribution to the observed gamma-ray flux. The likelihood function is defined as

$$L(\boldsymbol{\mu}|\mathbf{c}) = \Pi_{i=i_0,...,i_1} P_{\mu_i}(c_i), \tag{2.5}$$

where, for each energy bin i, μ_i and c_i denote the expected and observed count numbers, respectively, and $P_\mu(k) = \mu^k e^{-\mu}/k!$ is the Poisson probability mass function with mean value μ. The data are modeled by a simple power law with a spectral index $-\gamma$ and a normalization β, plus a line signal at fixed energy E_γ with the normalization α. The power law background is supposed to take into account not only the gamma-ray flux of astrophysical origin, but also the gamma-ray continuum which might be produced in the dark matter annihilation or decay additionally to the sharp gamma-ray line. Since the power law is only locally a good approximation to the background fluxes, we use a sliding energy window in the fitting procedure. For gamma-ray energies $E_\gamma \lesssim 10\,\text{GeV}$ we only take into account the energy bins $i \in [i_0, i_1]$ that lie within $\pm 2\sigma_{\Delta E}^{68\%}$ around E_γ, whereas, due to limited statistics, at high energies $E_\gamma \gtrsim 100\,\text{GeV}$ bins within a wider energy window from roughly $\frac{1}{3}E_\gamma$ to $3E_\gamma$ are considered. In the range $10\,\text{GeV} \lesssim E_\gamma \lesssim 100\,\text{GeV}$ the energy window size is interpolated between these two cases. Furthermore, events above $300\,\text{GeV}$ are always excluded from the analysis, which leads to energy windows asymmetric around the highest gamma-ray line energies. The expected number of counts in each energy bin is given by

$$\mu_i(\alpha, \beta, \gamma) = \int_{E_i^-}^{E_i^+} dE' \left(\beta \mathcal{E}_{\text{int}}(E') E'^{-\gamma} + \alpha \mathcal{E}_{\text{int}}(E_\gamma) \mathcal{D}(E', E_\gamma) \right), \tag{2.6}$$

where the $E_i^\pm$ denote the boundaries of each energy bin i, $\mathcal{E}_{\text{int}}$ is the energy dependent integrated total exposure, and we neglect the effects of the energy dispersion on the power-law background flux. To obtain $\mathcal{E}_{\text{int}}$, we integrate the exposure maps, which we derived with the Fermi Science Tools,[6] over the observed region of the sky, weighted by the angular profile of the expected gamma-ray line signal from dark matter decaying or annihilating inside the Galactic halo. The resulting integrated exposures are practically identical for decaying and annihilating dark matter signals, and are shown in the left panel of figure 2 for the halo and center regions. They can be approximated by $\mathcal{E}_{\text{int}}(E) \simeq \langle \mathcal{E}(E) \rangle \Delta\Omega$, where the target region averaged exposures are in the range $\langle \mathcal{E}(E) \rangle \simeq 5$–$8 \times 10^{10}\,\text{cm}^2\,\text{s}$, and $\Delta\Omega = 10.4\,\text{sr}$ $(1.30\,\text{sr})$ is the solid angle spanned by the halo (center) region. The observed differential gamma-ray fluxes for both target regions, as inferred from the exposure and count maps, are shown in the right panel of figure 2.

Depending on whether the normalization α of the gamma-ray line is kept free or fixed, the likelihood function in eq. (2.5) must be maximized with respect to three or two parameters, respectively:

$$L(\mathbf{c}) = \sup\{L(\boldsymbol{\mu}|\mathbf{c}) : \alpha, \beta, \gamma \in \mathbb{R}^+\} \qquad \text{or} \qquad L_\alpha(\mathbf{c}) = \sup\{L(\boldsymbol{\mu}|\mathbf{c}) : \beta, \gamma \in \mathbb{R}^+\}. \tag{2.7}$$

Defining $\Lambda_\alpha(\mathbf{c}) \equiv L_\alpha(\mathbf{c})/L(\mathbf{c})$, the 95% C.L. interval upper limit of the gamma-ray line normalization is given by the largest value of α which satisfies $-2\log\Lambda_\alpha(\mathbf{c}) \leq 4$. The parameter α is defined such that it can be directly identified with the corresponding gamma-ray line

---

[6]In `gtltcube` we use a zenith cut `zmax=105` to properly calculate the exposure also in cases where the field-of-view of the satellite intersects with the Earth's Albedo. However, due to our above cut on the satellite rocking angle (see footnote 4) this has only a small effect on the total exposure.
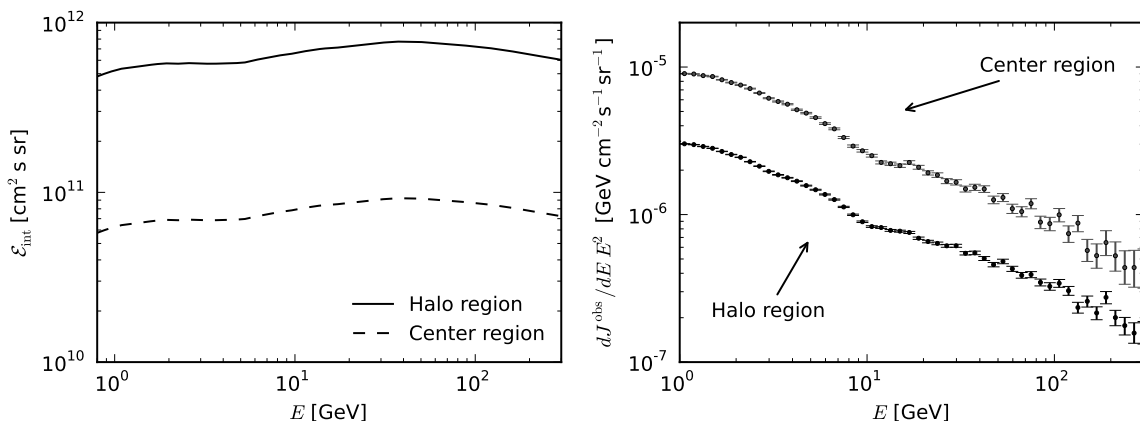
Figure 2. *Left panel*: integrated exposures $\mathcal{E}_{\text{int}}$ for both target regions, following the weighting method described in the text. *Right panel*: differential gamma-ray flux as observed in the two target regions.

flux, i.e. $J_\gamma \equiv \alpha$. In the absence of a gamma-ray line signal at the 5σ level, which would correspond to $-2\log\Lambda_{\alpha=0}(\mathbf{c}) \geq 23.7$, we quote the upper limit of the 95% C.L. interval as the upper limit on the gamma-ray line flux. Note that the $-2\log\Lambda_{\alpha=0}$ value corresponding to a 5σ-confidence level slightly deviates from the naively expected 25, because the normalization of the gamma-ray line is bounded from below, i.e. $\alpha \geq 0$. The adopted value can be derived by recognizing that in absence of a gamma-ray line in 50% of the cases the optimal fit would actually require an unphysical negative normalization of the gamma-ray line, since for large enough count numbers statistical fluctuations are symmetric around their mean. These cases yield $-2\log\Lambda_{\alpha=0} = 0$, whereas in the other 50% of the cases, the $-2\log\Lambda_{\alpha=0}$ would follow a conventional χ^2-distribution with one degree of freedom.[7]

The likelihood analysis is performed using PyFITS[8] and PyMinuit, an interface to the function minimizer MINUIT 1.7.9.[9]

2.2 Results

No gamma-ray lines with 5σ significance are found in the 1–300 GeV energy range. Details and caveats of the analysis are discussed in section 2.3. Our results for the 95% and 99.7% C.L. limits on the gamma-ray line flux are shown in figure 3 as a function of the gamma-ray line energy for both halo and center regions. As discussed in section 2.3, instrumental effects forbid us to take these limits at face value; the conservative limits summarized in table 3 should be used instead. These are derived by quoting the weakest limit we obtain in given energy bands. Together with eqs. (2.1) and (2.2), it is then straightforward to derive the corresponding constraints on the dark matter decay width or annihilation cross section.

Limits on the inverse dark matter decay width into monochromatic photons and neutrinos, $\Gamma^{-1}_{\psi\to\gamma\nu}$, as derived from the halo region observations, are presented in figure 4, assuming

---

[7]We confirmed this behavior with a Monte Carlo analysis. Details about the likelihood-ratio and confidence intervals can be found e.g. in refs. [82, 83]. Note that we do not use a "trial factor" as discussed in refs. [76, 84], which only becomes relevant when constraining models that predict a multitude of lines or when claiming a line discovery.

[8]PyFITS is a product of the Space Telescope Science Institute, which is operated by AURA for NASA, see http://www.stsci.edu/resources/software_hardware/pyfits.

[9]See http://code.google.com/p/pyminuit/ and http://seal.web.cern.ch/seal/snapshot/work-packages/mathlibs/minuit/.
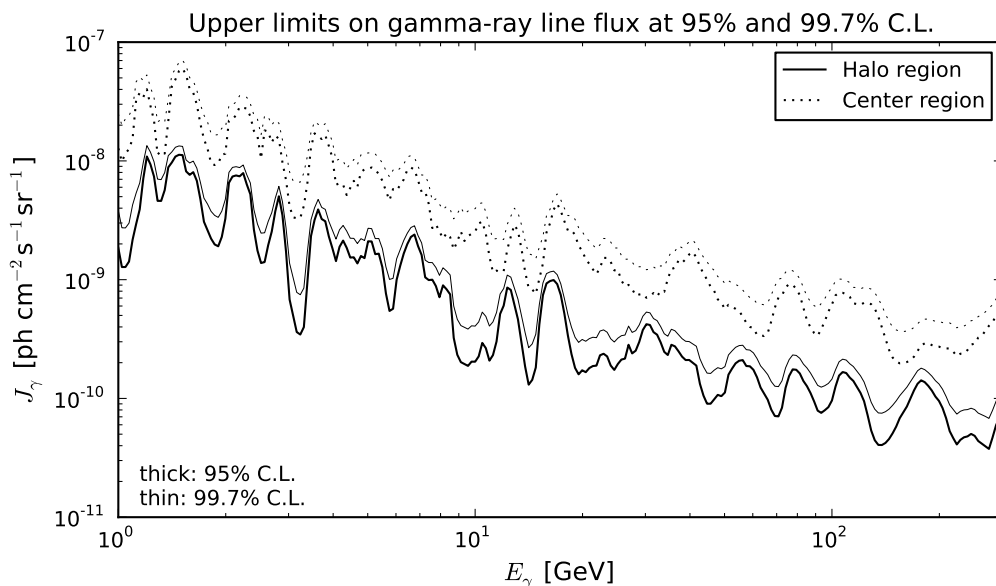
Figure 3. Our results for the 95% and 99.7% C.L. upper limits on the monochromatic photon flux from the halo and the center regions, as function of the gamma-ray line energy E_γ. Note that due to instrumental effects these limits are expected to be too strong at lower energies in some cases (cf. section 2.3). The corresponding conservative limits are show in table 3 (as well as in the figures 4 and 5).

Target region	$\Gamma^{\text{profile}}_{\psi \to \gamma\nu}/\Gamma_{\psi \to \gamma\nu}$			$\langle\sigma v\rangle^{\text{profile}}_{\psi\psi \to \gamma\gamma}/\langle\sigma v\rangle_{\psi\psi \to \gamma\gamma}$		
	Iso.	NFW	Ein.	Iso.	NFW	Ein.
Halo	0.96	1.00	1.00	1.03	1.00	0.89
Center	1.03	1.00	0.91	1.65	1.00	0.64

Table 2. Rescaling factors for the bounds on the dark matter decay width and annihilation cross section (shown in table 3), corresponding to the different halo profiles. In most cases, the weakest bounds are obtained for the isothermal profile (Iso.), the strongest bounds for the Einasto profile (Ein.), whereas the NFW profile leads to intermediate constraints.

a NFW dark matter profile. The gray line shows the bounds as they directly follow from the flux limits in figure 3. In most of the considered energy range, they fluctuate around 10^{29} s. The slight improvement with respect to the previous Fermi LAT limits [52] (dashed line) is due to the increased statistics after two years of data taking. The black dots represent the weakest limits obtained when varying the gamma-ray line energy within different adopted energy bands. Except at the highest energies, these values fluctuate around 6×10^{28} s, and are summarized in table 3. Adopting halo profiles different from the NFW profile would change the limits by a few percent. The corresponding rescaling factors for the Einasto and the isothermal profiles are summarized in table 2, and their impact on the limits is illustrated by the blue bands in figure 4. Note that the normalization of the dark matter profile at Sun's position is another source of uncertainty, which is not captured in the rescaling parameters of table 2. We do not plot the somewhat weaker limits on the decay width obtained from the center region, which can be found in table 3 for completeness.

In figure 5 we present the limits on the dark matter annihilation cross section into
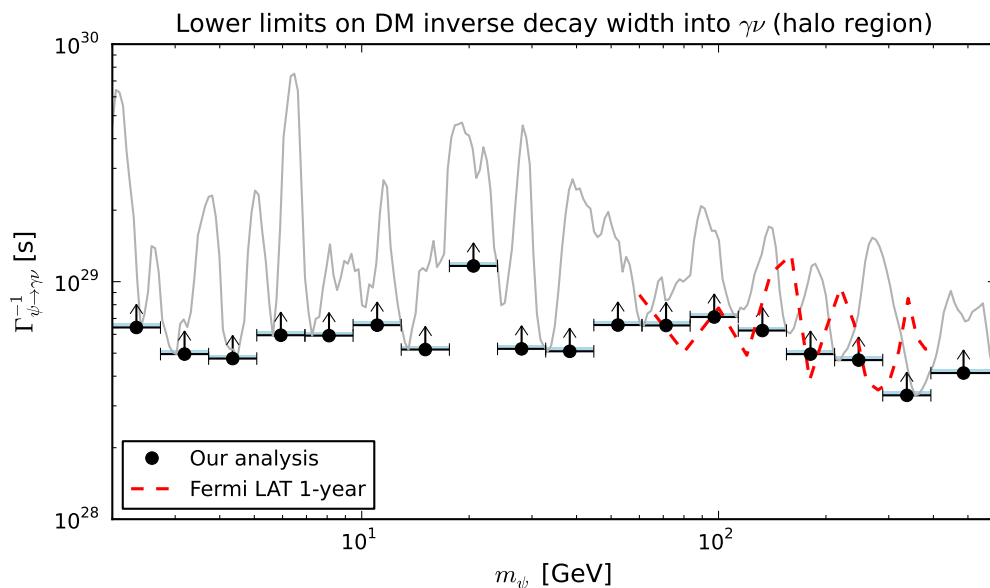
Figure 4. Lower bounds on the dark matter inverse decay width into monochromatic photons and neutrinos, $\Gamma^{-1}_{\psi \to \gamma\nu}$, as a function of the dark matter mass m_ψ, derived from the halo region fluxes assuming the NFW dark matter profile. The gray-solid line shows the 95% C.L. limits as directly derived from the line flux limits shown in figure 3. The black dots show the weakest limits obtained in the adopted energy bands and are listed in table 3. For comparison, the previous Fermi LAT limits from ref. [52] are also shown by the red-dashed line (rescaled to our decay channel). The barely visible blue bands illustrate how the bounds change when using the isothermal or Einasto dark matter profiles instead.

gamma-ray pairs, $\langle \sigma v \rangle_{\psi\psi \to \gamma\gamma}$, as derived from the center region observations. As illustrated by the blue band, the uncertainties coming from the dark matter density profile are much larger than in the case of dark matter decay and of the order of $\sim 50\%$, cf. table 2. For comparison, we also show the previous limits obtained by EGRET [53].[10] The present analysis improves these limits by up to an order of magnitude, which is essentially due to the increased statistics of Fermi LAT with respect to EGRET. Furthermore, at high energies, we slightly strengthen the previous Fermi LAT constraints [52]. Our results are summarized in table 3. It is interesting to note that, assuming the NFW profile, the limits on the dark matter annihilation cross section derived from the halo region are only a factor ~ 2 weaker than the limits derived from the center region.

Using kinematic considerations, our results can be straightforwardly translated into constraints on two-body decay or annihilation into a monochromatic photon plus a massive neutral particle N with mass m_N. This is relevant for the common case of annihilation/decay into γZ^0. However, in principle m_N is a free parameter, and if m_N is close to the dark matter mass m_ψ, the line signal can be even strongly enhanced in some scenarios [50]. Defining the quantity

$$x \equiv 1 + \sqrt{1 + \frac{m_N^2}{E_\gamma^2}}, \qquad (2.8)$$

---

[10]Note that the cross section limits shown in figure 8 of ref. [53] are incorrectly too strong by a factor of ten, whereas the flux limits presented in figure 7 are correct [priv. comm. with the authors]. The EGRET cross section limits that we present in figure 5 are derived from figure 7 of ref. [53].
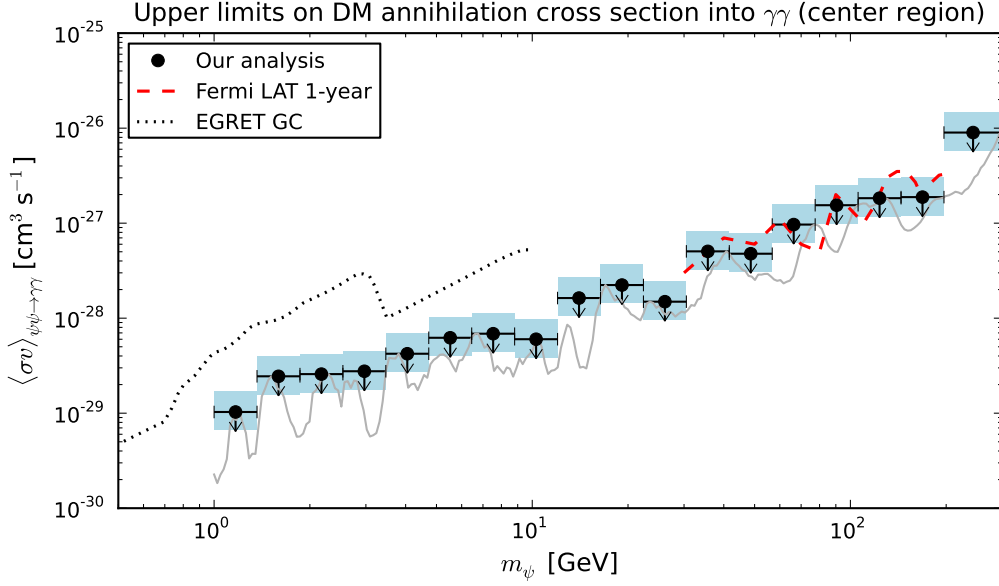
Figure 5. Upper bounds on the annihilation cross section into gamma-pairs, $\langle\sigma v\rangle_{\psi\psi\to\gamma\gamma}$, as a function of the dark matter mass m_ψ, derived from the center region fluxes assuming the NFW dark matter profile. The gray-solid line shows the 95% C.L. limits as directly derived from the line flux limits shown in figure 3. The black dots show the weakest limits obtained in the adopted energy bands and are listed in table 3. For comparison, the previous Fermi LAT limits from ref. [52] as well as the limits derived from EGRET observations of the Galactic center [53] are also shown by the red-dashed and the black-dotted lines, respectively. The blue bands illustrate how the bounds change when using the isothermal or Einasto dark matter profiles instead.

which is bounded from below by $x \geq 2$, our limits for the decay into $\gamma\nu$ translate into limits on the decay into γN via

$$\Gamma_{\psi\to\gamma N}(m_\psi) = \frac{x}{2}\,\Gamma_{\psi\to\gamma\nu}(E_\gamma)\,, \qquad \text{where} \quad m_\psi = x\,E_\gamma\,. \tag{2.9}$$

For the annihilation scenario the cross section limits on $\psi\psi \to \gamma N$ are obtained by

$$\langle\sigma v\rangle_{\psi\psi\to\gamma N}(m_\psi) = \frac{x^2}{2}\,\langle\sigma v\rangle_{\psi\psi\to\gamma\gamma}(E_\gamma)\,, \qquad \text{where} \quad m_\psi = \frac{x}{2}\,E_\gamma\,. \tag{2.10}$$

Models that are partially constrained by our limits include singlet dark matter [17] and SU(2) vector dark matter [46], but also refs. [19–22, 50]. Scenarios that remain practically unconstrained include the standard MSSM scenario [9], but also refs. [15, 16, 23–25]. The particular case of gravitino dark matter will be discussed in the next section.

2.3 Discussion

One crucial assumption underlying our analysis is that the background flux in the different considered energy windows can be well approximated by a power-law. This assumption is most likely to break down in cases where the statistics is very good. In order to check the validity of a power-law ansatz, we show in figure 6 the χ^2/d.o.f. of the background-only (green lines) and of the background-plus-signal (red lines) fits, as function of the gamma-ray line
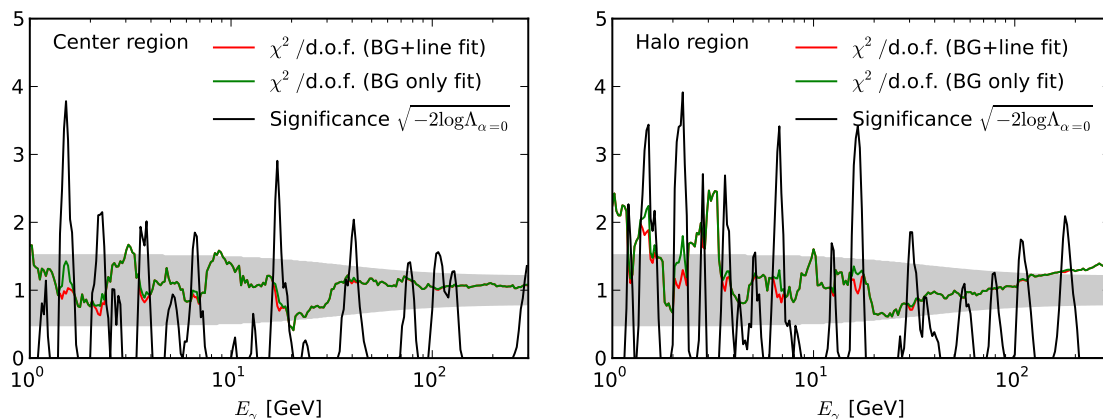
Figure 6. Significance of a potential line signal (black line) in the center (left panel) and halo (right panel) regions in terms of standard deviations. We also show the χ^2/d.o.f. values of fits with (red line) and without (green line) line signal. The gray shaded area corresponds to a p-values of $\geq 5\%$. Especially at low energies in the halo region, significant deviations occur from what is statistically expected in absence of a signal, as discussed in section 2.3.

energy.[11] The grey band corresponds to a *p*-value of $\geq 5\%$. For the center region the fits are essentially in agreement with the data over the whole energy range. However, *p*-values significantly smaller than 5% occur at energies between 1 and 10 GeV (as well as at high energies close to 300 GeV) when considering the halo region, which has a three times larger statistics than the center region. Assuming that the astrophysical gamma-ray fluxes follow smooth bended power-laws, this tension points to an instrumental effect, presumably related to the energy reconstruction of gamma-ray events.

The black lines in figure 6 show the significance (in terms of standard deviations) of line signals with respect to a power-law background. Over the whole energy range we are performing $\mathcal{O}(50)$ statistically independent tests for a line. Hence, we expect to see a few cases with 2σ significance, and practically no case with 3σ significance. This expectation is marginally compatible with the observations of the center region, and is clearly violated for the halo region, where four $> 3\sigma$ excesses are observed below 20 GeV. However, an interpretation of these excesses in terms of gamma-ray lines would be suspicious: they occur at low energies in the halo region, where the statistics is best and hence the impact of instrumental effects most relevant, as indeed indicated by the bad χ^2/d.o.f. of the background-fits at this energy range. Moreover, most line-like features appear, although with a different significance, at the same position in both, the halo and the center region, indicating again a systematic effect. Without further understanding and reduction of instrumental effects, no conclusive statement about the existence of gamma-ray lines (below $\sim 5\sigma$ significance) in this energy range can be made.

The limits presented in figures 4, 5 and table 3 are conservative in the sense that we always quote the weakest limit we obtain in given energy bands. Especially in the halo region at energies below 20 GeV, this ensures that our limits are dominated (and weakened) by the presence of the line-like artefacts in the energy spectrum. A future removal of these artefacts from the data is expected to lead in general to a strengthening of the presented limits. Note

---

[11]The smallness of the differences between the χ^2/d.o.f. of the background-plus-signal and background-only fit at high energies comes from the fact that the χ^2 values are actually dominated by the background and not by the narrow signal.
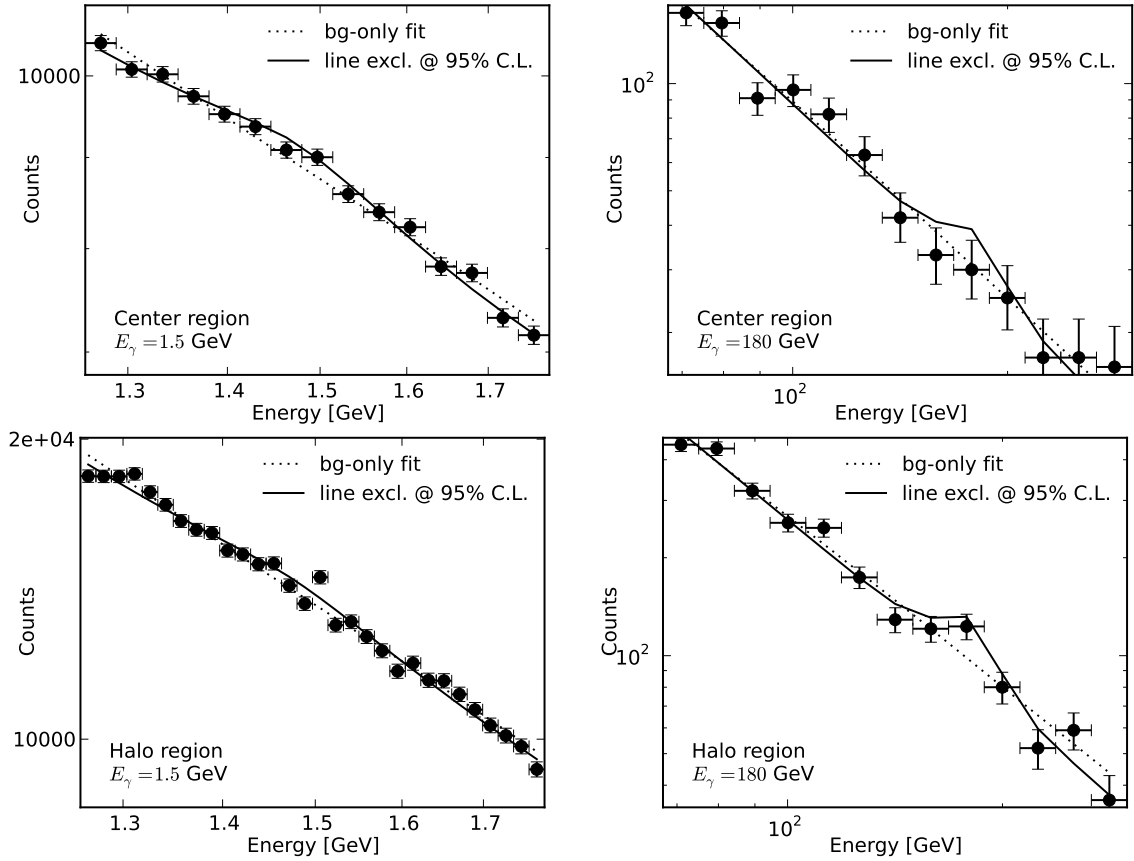
Figure 7. Line signals that are excluded at 95% C.L. (solid line), compared to best-fit background-only model (dotted line) and data. We show results for the center (top panels) and halo (bottom panels) region. The gamma-ray line energies are $E_\gamma = 1.5\,\text{GeV}$ (left panels) and $E_\gamma = 180\,\text{GeV}$ (right panels). In the left panels, the signal-to-background ratio is 2.6% (top) and 1.5% (bottom).

that the presence of a real gamma-ray line signal significantly stronger than the artefacts would have lead to limits dominated by the line signal itself.

For two different gamma-ray line energies and for both center and halo regions, we show in figure 7 the line signals that are excluded at 95% C.L. (for which $-2\log\Lambda_\alpha(\mathbf{c}) = 4$, see above), and compare them with the best-fit background-only fluxes. The gamma-ray line energies are chosen such that the corresponding limits dominate in their respective energy bands in case of the halo region. Furthermore, the energy ranges shown in the plots correspond to the energy windows used in the fitting procedure, and we rebinned the data for better visibility. At low energies the gamma-ray line constraints essentially come from the non-observation of a strong bending in the measured energy spectrum (with signal-to-background ratios as small as 1.5%), whereas at high energies, where the considered energy window is larger, the constraints come from the non-observation of a well defined bump.

In summary, due to the apparent presence of line-like artefacts at the few percent level in the energy spectrum of the public 'DataClean' event class of the Fermi LAT, the flux limits from figure 3 are expected to be too strong in some cases, especially at energies below $\sim 20\,\text{GeV}$. Instead, the limits presented in figure 4, 5 and table 3 should be used.

Further more general uncertainties and systematic effects enter our analysis [76, 77]:

E_γ [GeV]	J_γ [ph/(cm^2 s sr)]		$\Gamma^{-1}_{\psi\to\gamma\nu}$ [s]		$\langle\sigma v\rangle_{\psi\psi\to\gamma\gamma}$ [cm^3 s^{-1}]	
	halo $\times 10^{-9}$	center $\times 10^{-9}$	halo $\times 10^{28}$	center $\times 10^{28}$	halo $\times 10^{-28}$	center $\times 10^{-28}$
1.0–1.4	11	40	6.4	4.4	0.25	0.10
1.4–1.9	11	60	5.0	2.3	0.41	0.24
1.9–2.5	7.9	29	4.7	3.3	0.63	0.26
2.5–3.5	5.0	18	5.9	4.6	0.63	0.22
3.5–4.7	3.9	17	5.9	3.4	0.82	0.42
4.7–6.5	2.1	8.8	6.6	4.7	1.3	0.49
6.5–8.8	2.4	8.8	5.2	3.6	1.7	0.69
8.8–12	0.60	3.1	12	6.6	1.4	0.60
12–16	0.98	3.0	5.2	4.4	4.2	1.4
16–22	0.99	4.4	5.1	2.9	4.4	2.2
22–31	0.42	1.5	6.6	5.9	6.2	1.5
42	0.42	1.7	6.5	3.0	6.3	5.1
42–57	0.21	1.5	7.1	3.3	11	4.8
57–77	0.20	0.92	6.2	3.0	17	9.4
77–106	0.18	0.90	5.0	2.6	29	15
106–144	0.17	0.78	4.7	2.6	31	18
144–197	0.14	0.29	3.3	3.9	72	18
197–300	0.10	0.59	4.1	1.2	96	91

Table 3. Conservative upper limits on the flux in gamma-ray lines J_γ, as well as on the decay width $\Gamma_{\psi\to\gamma\nu}$ and the annihilation cross section $\langle\sigma v\rangle_{\psi\psi\to\gamma\gamma}$ of dark matter into monochromatic photons, for line energies $E_\gamma = 1$–300 GeV. In each of the indicated energy bands, we varied E_γ to find the weakest possible 95% C.L. limit. The flux limits for all values of E_γ are shown in figure 3 (see also section 2.3). The limits are evaluated for the halo and for the center region separately, and hold for the NFW profile. Other dark matter profiles just require a rescaling of the bounds as shown in table 2.

the systematic uncertainties in the effective area are energy dependent and increase from 5% at 560 MeV to 20% at 10–100 GeV in case of the 'DataClean' event class [54] (note that these uncertainties amount mainly to an overall shift in the effective area). Uncertainties on the level of around 20% are expected to continue up to energies of hundreds of GeV [76, 77], but one has to keep in mind that a precise determination of the effective area at these high energies is still lacking due to limited statistics. However, even values reasonably larger than 20% would only mildly affect our conclusions. Over the whole considered energy range, the systematics of the LAT effective area consequently translate into uncertainties for our dark matter limits that range between 5% and $\sim$ 20%. The absolute energy scale of the Fermi LAT is determined up to $^{+5\%}_{-10\%}$ [48]. This translates into an additional uncertainty on the dark matter annihilation cross section $\langle\sigma v\rangle_{\psi\psi\to\gamma\gamma}$ of $^{+10\%}_{-20\%}$, and on the decay width $\Gamma_{\psi\to\gamma\nu}$ of $^{+5\%}_{-10\%}$, respectively.

Finally, we have also checked that when extending our analysis to 500 GeV no significant line signals at high energies are revealed, and the limits below the highest energy band presented in table 3 are only marginally affected. Considering the 197–300 GeV (300–500 GeV) energy band, we obtain in this case $\Gamma^{-1}_{\psi\to\gamma\nu} > 6.0 \times 10^{28}$ s (1.7×10^{28} s) for the halo region,

and $\langle\sigma v\rangle_{\psi\psi\to\gamma\gamma} < 4.1\times 10^{-27}$ cm^3 s^{-1} (1.54×10^{-26} cm^3 s^{-1}) for the center region. However, we emphasize that energies above $300\,\mathrm{GeV}$ lie outside of the nominal energy range of the Fermi LAT.

3   Consequences for gravitino dark matter

Local extensions of the supersymmetric standard model predict the existence of the gravitino, the supersymmetric partner of the graviton. Depending on the mechanism of supersymmetry breaking, it can be the lightest superparticle (LSP). In this case, it provides a natural dark matter candidate [85], and is an interesting alternative to the standard WIMP scenario.

The dominant contribution to the gravitino production in the early Universe comes from the 2-to-2 QCD scatterings, which are taking place in the thermal bath at reheating. The resulting energy density is given by

$$\Omega_{3/2}^{\mathrm{th}}\, h^2 = C \left(\frac{100\,\mathrm{GeV}}{m_{3/2}}\right)\left(\frac{m_{\tilde{g}}}{1\,\mathrm{TeV}}\right)^2\left(\frac{T_R}{10^{10}\,\mathrm{GeV}}\right), \tag{3.1}$$

where T_R is the reheating temperature, while $m_{3/2}$ and $m_{\tilde{g}}$ are the gravitino and gluino masses, respectively. To leading order in the gauge couplings, $C \simeq 0.5$ [86–88].[12] Remarkably, the observed dark matter relic density $\Omega_{\mathrm{DM}}h^2 = 0.11$ [89] is obtained for typical supersymmetric parameters, $m_{3/2} \sim 100\,\mathrm{GeV}$ and $m_{\tilde{g}} \sim 1\,\mathrm{TeV}$, and for reheating temperatures $T_R \sim 10^{10}\,\mathrm{TeV}$ as required for thermal leptogenesis to generate the observed baryon asymmetry [90, 91].

However, the above scenario is not free of problems: if R-parity is conserved, the decay of the next-to-lightest supersymmetric particle (NLSP) into gravitino and standard model particles is suppressed by the Planck scale. As a consequence, the NLSP becomes very long-lived and can dramatically affect the successful prediction of the standard big bang nucleosynthesis (BBN) scenario [92–98]. Several alternative scenarios have been proposed to consistently accommodate thermal leptogenesis, gravitino dark matter and BBN, like assuming sneutrino [99] or stop [100] NLSPs, diluting the NLSP abundance by entropy production [101], or introducing new NLSP decay channels into hidden sector states [102, 103]. Also, the reheating temperature can be considerably reduced by considering non-thermal leptogenesis scenarios, as for example recently proposed in mechanisms where the universe is reheated through the decay of non-relativistic right-handed neutrinos produced in false vacuum decay [104, 105].

Alternatively, it has been proposed that R-parity could be mildly violated [30]. Such a violation could be e.g. produced by dynamical breaking of $\mathrm{U}(1)_{B-L}$ at low scales in the hidden sector [106]. It would lead to a rapid decay of the NLSP before the onset of BBN, thus rendering its impact on the standard cosmological picture negligible. Notably, even though the gravitino is not stable anymore in such a case, it still constitutes a viable dark matter candidate because its decay into standard model particles is doubly suppressed by the small R-parity breaking parameter as well as by the Planck mass [31], leading to lifetimes longer than the age of the Universe.

This R-parity violating scenario is particularly attractive because it opens up the possibility to probe gravitino dark matter by searching for its decay products in the cosmic-ray

---

[12]Note that C has $\mathcal{O}(1)$ uncertainty due to unknown higher order contributions and nonperturbative effects [86].

fluxes. In addition to cosmic anti-matter [35, 36] and neutrino [38] fluxes, the produced gamma-ray flux [30–34, 36] is of high interest because, besides the continuous component generated by the fragmentation of the Higgs and gauge bosons, the gamma-ray energy spectrum typically features an intense line, arising from the $\psi_{3/2} \to \gamma\nu$ two-body decay already at tree level.

In the rest of this section, we will apply the above Fermi LAT limits on gamma-ray lines to the decaying gravitino scenario. First, we will summarize the relevant aspects of bilinear R-parity violation, which will form the theoretical framework of our analysis. Second, we will present limits on the size of R-parity violation, and discuss prospect for seeing long-lived neutralino and stau NLSPs at the LHC, extending the analysis made in [107].

3.1 R-parity breaking model

The supersymmetric standard model with bilinear R-parity breaking is, in addition to the standard $\mathrm{SU}(3)_c \times \mathrm{SU}(2)_L \times \mathrm{U}(1)_Y$ gauge interactions, defined by mass-mixing terms between lepton and Higgs fields in the superpotential

$$W = W_{\mathrm{MSSM}} + \mu_i H_u l_i \,, \tag{3.2}$$

as well as by the mass-mixing terms in the scalar potential as induced by supersymmetry breaking

$$\mathcal{L} = \mathcal{L}_{\mathrm{soft}}^{\mathrm{MSSM}} + B_i H_u \tilde{l}_i + m_{id}^2 \, \tilde{l}_i^\dagger H_d + \mathrm{h.c.} \,. \tag{3.3}$$

Here, W_{MSSM} and $\mathcal{L}_{\mathrm{soft}}^{\mathrm{MSSM}}$ are the usual R-parity conserving MSSM superpotential and scalar Lagrangian, $H_{u/d}$ are the up/down-type Higgs doublets, l_i the lepton doublets, and μ_i, B_i and m_{id}^2 are the R-parity violating couplings. As proposed in ref. [107], it is convenient to work in a lepton-higgs basis where the mass mixings μ_i, B_i and m_{id}^2 are traded for R-parity breaking Yukawa couplings. This can be achieved by a supersymmetric rotation of the superfields, followed by a non-supersymmetric rotation of the scalar fields alone. Besides the R-parity breaking Yukawa couplings, which will become relevant for the decay of the stau NLSP below, these rotations also generate mass-mixing terms between the neutralinos and the neutrinos. This neutrino-neutralino mixing, which can be parameterized by the dimensionless parameter ζ, finally induces the gravitino decay mode $\psi_{3/2} \to \gamma\nu$ as well as the decay of neutralino NLSPs (see ref. [107] for a definition of ζ in terms of the bilinear R-parity violating couplings μ_i, B_i and m_{id}^2).

We will consider two typical sets of boundary conditions for the supersymmetry breaking parameters of the MSSM at the grand unification (GUT) scale for definiteness. The first one corresponds to equal scalar and gaugino masses

$$(\mathrm{A}) \qquad m_0 = m_{1/2} \,, \qquad a_0 = 0 \,, \qquad \tan\beta = 10 \,, \tag{3.4}$$

for which the bino-like neutralino χ_1^0 is the NLSP. In the second one, which corresponds to no-scale models or gaugino mediation,

$$(\mathrm{B}) \qquad m_0 = 0 \,, \qquad m_{1/2} \,, \qquad a_0 = 0 \,, \qquad \tan\beta = 10 \,, \tag{3.5}$$

the lightest stau $\tilde{\tau}_1$ is the NLSP. In both cases, $\tan\beta = 10$ has been chosen as a representative value, and the trilinear scalar coupling a_0 has been set to zero for simplicity. The universal

gaugino mass $m_{1/2}$ remains as the only independent variable. For both sets of boundary conditions, the gaugino masses $M_{1,2,3}$ satisfy the following relations at the electroweak scale

$$\frac{M_3}{M_1} \simeq 5.9\,, \qquad \frac{M_2}{M_1} \simeq 1.9\,. \tag{3.6}$$

Electroweak precision tests (EWPT) yield important lower bounds on the superparticle mass spectrum [88]. For a neutralino NLSP, the most stringent constraint comes from the Higgs potential. The universal gaugino mass $m_{1/2}$ is required to be high enough in order for the Higgs mass to fulfills the LEP lower bound $m_h > 114.4\,\text{GeV}$ [108]. This implies the lower limit $m_{\chi_1^0} \gtrsim 130\,\text{GeV}$.[13] However, allowing negative a_0 or scalar masses much larger than $m_{1/2}$ at the GUT scale would weaken this limit, and we will take $m_{\chi_1^0} > 100\,\text{GeV}$ as a lower bound for the neutralino mass subsequently. In the stau NLSP case, the lower bound comes from the absence of pair production of heavy charged particles at LEP and reads $m_{\tilde{\tau}_1} > 100\,\text{GeV}$ [108].

For a typical effective neutrino mass $\widetilde{m}_1 = 10^{-3}\,\text{eV}$, successful thermal leptogenesis requires a minimal reheating temperature of $T_R \sim 10^9\,\text{GeV}$ [91]. Using eq. (3.1) together with a lower bound on the gluino mass $m_{\tilde{g}} \gtrsim 500\,\text{GeV}$ [109], this implies a lower bound for the gravitino mass $m_{3/2} \gtrsim 5\,\text{GeV}$.

In addition to the lower limits, NLSP mass upper limits follow from the requirement that the gravitino does not overclose the Universe. Indeed by rewriting eq. (3.1) one obtains the constraint

$$m_{\text{NLSP}} \simeq 310\,\text{GeV} \left(\frac{\xi}{0.2}\right) \left(\frac{m_{3/2}}{100\,\text{GeV}}\right)^{1/2} \left(\frac{10^9\,\text{GeV}}{T_R}\right)^{1/2}, \tag{3.7}$$

where $\xi \equiv m_{\text{NLSP}}/m_{\tilde{g}}$ is implicitly fixed by the supersymmetry breaking boundary conditions [88]. Since $m_{\text{NLSP}} \propto m_{3/2}^{1/2}$, requiring the gravitino to be the LSP induces absolute upper bounds on the NLSP masses. In the case of the neutralino NLSP, eq. (3.7) implies $m_{\chi_1^0} \lesssim 690\,\text{GeV}$ for $\xi = 1/5.9$, and is essentially independent of m_0 and $\tan\beta$. For the stau NLSP, $\tan\beta = 10$ yields $\xi = 1/6.2$, which consequently leads to the more stringent bounds $m_{\tilde{\tau}_1} \lesssim 615\,\text{GeV}$. Note that there is a strong dependence on $\tan\beta$ in that case [88], and that ξ decreases with increasing $\tan\beta$.

3.2 Fermi LAT constraints on the NLSP decay length

The gravitino decay mode relevant for the discussion in this paper is the decay into photons and neutrinos via $\psi_{3/2} \to \gamma\nu$. However, decays into $W^\pm \ell^\pm$, $Z^0\nu$ and $h^0\nu$ final states are also possible, and have often large branching ratios. Below the corresponding kinematic thresholds, three-body decay with intermediate massive gauge bosons can become important in some cases [42].

Additionally to the gamma-ray line from $\psi_{3/2} \to \gamma\nu$, the different decay modes will produce a gamma-ray continuum, coming from Higgs and gauge boson fragmentation as well as from final state radiation of the charged leptons. This continuous spectrum has a cutoff at the position of the gamma-ray line, namely at half of the gravitino mass. Since we required in the above line search that all gamma-ray fluxes except the line follow a power-law locally around the line's energy (cf. section 2.1), a too large continuum contribution from gravitino decay would render our line search strategy invalid. We expect this to become relevant for

---

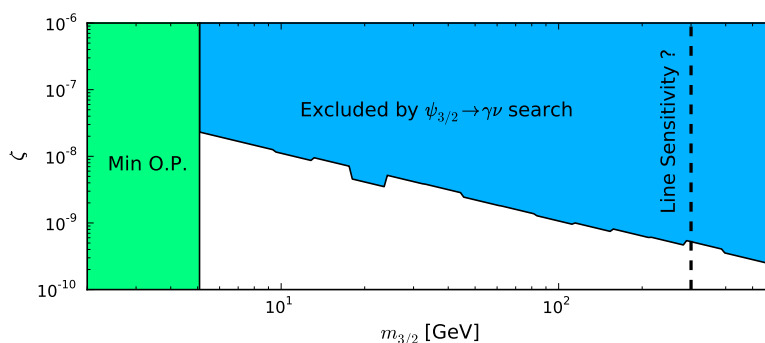[13]Note that $m_{\chi_1^0} \simeq M_1$ with good accuracy [107].

Figure 8. Upper bounds on the R-parity violation parameter ζ, derived from the Fermi LAT gamma-ray line limits in figure 4. For thermal leptogenesis, overproduction (O.P.) of gravitinos already excludes the left green region. As discussed in the text, the adopted strategy for line searches might fail for gravitino masses above a few hundred GeV (dashed black line).

branching ratios into gamma-ray lines below $10^{-3} \ldots 10^{-2}$, and postpone a detailed analysis of this effect to future work. Using the branching ratios presented in refs. [36, 38], we find that this problem can become severe for gravitino masses above a few hundred GeV, $m_{3/2} \gtrsim 300 \, \text{GeV}$. However, one has to keep in mind that the exact branching ratio into lines is in principle model-dependent. In what follows we assume for simplicity that no continuum contribution disturbs our line search, and we present limits over the full range of accessible gravitino masses.

The gravitino inverse decay rate into photon/neutrino pairs is given by[14] [31, 107]

$$\Gamma_{\psi_{3/2}\to\gamma\nu}^{-1} = \frac{32\sqrt{2}}{\alpha\zeta^2} \frac{G_{\mathrm{F}}M_{\mathrm{P}}^2}{m_{3/2}^3} \frac{M_1^2 M_2^2}{(M_2 - M_1)^2} \left(1 + \mathcal{O}\left(s_{2\beta}\frac{m_Z^2}{\mu^2}\right)\right), \tag{3.8}$$

where α is the electromagnetic fine structure constant, $M_{\mathrm{P}} = 2.4 \times 10^{18} \, \text{GeV}$ the reduced Planck mass, and $G_{\mathrm{F}} = 1.16 \times 10^{-5} \, \text{GeV}^{-2}$ is the Fermi constant. Using this expression, the limits on the gamma-ray line flux can be translated into upper limits on the R-parity breaking parameter ζ. A conservative bound on ζ is obtained for a given gravitino mass when using the corresponding maximally allowed bino mass. The latter is obtained by combining eq. (3.1) and (3.6) considering the lowest reheating temperatures allowed in the thermal leptogenesis scenario, i.e. $T_R \sim 10^9 \, \text{GeV}$. The limits on the R-parity violation parameter ζ are presented in figure 8. As discussed above, for gravitino masses above a few hundred GeV, our line search may fail due to a too large gamma-ray continuum contribution, which is indicated by the dashed line. Note also that, at these high gravitino masses, the production of anti-protons in gauge boson fragmentation could further constrain the ζ parameter [35, 36]. The implications of our gamma-ray line limits on the decay of the NLSP are discussed next.

3.2.1 Stau NLSP

In the case of the $\tilde{\tau}_1$-NLSP, the total decay width of the lightest mass eigenstate is a mixture of left and right handed partial decays

$$\Gamma_{\tilde{\tau}_1} = \sin^2\theta_{\tilde{\tau}} \, \Gamma_{\tilde{\tau}_L} + \cos^2\theta_{\tilde{\tau}} \, \Gamma_{\tilde{\tau}_R} . \tag{3.9}$$

---

[14]The correction factor is less than 10% for bino masses under consideration [107].

Since the R-parity breaking Yukawa couplings are typically proportional to the ordinary Yukawa couplings, decays into second and third families dominate. For definiteness, we will below assume a flavor structure as described in ref. [107], which is based on a Froggatt-Nielsen $U(1)$ flavor symmetry. In such a framework, the chiral state decays are dominated by the following channels [107]

$$\tilde{\tau}_R \to \tau_L \nu, \mu_L \nu \,, \tag{3.10a}$$

$$\tilde{\tau}_L \to \bar{t}_R b_L \,. \tag{3.10b}$$

The corresponding decay rates are

$$\Gamma_{\tilde{\tau}_L} = \frac{\epsilon^2}{16\pi v^2} \frac{m_t^2}{m_{\tilde{\tau}_1}^3} \, 3 \, (m_{\tilde{\tau}_1}^2 - m_t^2 - m_b^2) \sqrt{[m_{\tilde{\tau}_1}^2 - (m_t + m_b)^2][m_{\tilde{\tau}_1}^2 - (m_t - m_b)^2]} \,, \tag{3.11a}$$

$$\Gamma_{\tilde{\tau}_R} = \frac{\epsilon^2}{16\pi v^2} \frac{m_t^2}{m_{\tilde{\tau}_1}^3} \, (\tan\beta)^2 \, (m_{\tilde{\tau}_1}^2 - m_\tau^2)^2 \,, \tag{3.11b}$$

where the dimensionless parameter ϵ is directly related to the R-parity violating Yukawa couplings (see ref. [107] for details). In principle ζ and ϵ are independent parameters because they stem from different linear combinations of the bilinear R-parity violating couplings μ_i, B_i and m_{id}^2. We choose $\zeta \simeq \epsilon$ in order to set limits on the stau decay length. However, one has to keep in mind that in principle ζ could be set to values much smaller than ϵ by a proper choice of the parameters μ_i, B_i and m_{id}^2. The behavior of the mixing angle $\theta_{\tilde{\tau}}$ with the stau mass $m_{\tilde{\tau}_1}$ can be deduced from the RGEs using the boundary conditions eq. (3.5).

Using the upper limits on the R-parity breaking parameter ζ from figure 8, we can derive lower bounds on the stau decay length. Our results are shown in figure 9. The parameter space is already constrained by EWPT and overproduction bounds, and the lower limits on the neutralino decay length vary between 100 m and 10 km. It is interesting that if such particle were to be produced at the LHC, a sizable amount of their decay could take place in the detector [37]. We obtain a lowest possible decay length $c\tau_{\tilde{\tau}} \simeq 85$ m for $m_{3/2} \simeq 16$ GeV and $m_{\tilde{\tau}_1} \simeq 100$ GeV.

3.2.2 Neutralino NLSP

A neutralino NLSP heavier than 100 GeV dominantly decays into $W^\pm \ell^\mp$ and $Z^0 \nu$ [110, 111]. The corresponding decay width is directly proportional to the R-parity breaking parameter ζ squared, which also enters the gravitino decay width in eq. (3.8). As a consequence, the two quantities can be related through [107]

$$\tau_{\chi_1^0} = \frac{c_w^2}{2\sqrt{2}} \frac{(M_2 - M_1)^2}{M_2^2} \frac{m_{3/2}^3}{G_{\rm F} M_{\rm P}^2 m_{\chi_1^0}^3} \frac{\Gamma_{\psi_{3/2} \to \gamma\nu}^{-1}}{2f(m_{\chi_1^0}, m_W) + f(m_{\chi_1^0}, m_Z)} \,, \tag{3.12}$$

where the phase space factor f is defined by

$$f(m_1, m_2) = \left(1 - \frac{m_2^2}{m_1^2}\right)^2 \left(1 + 2\frac{m_2^2}{m_1^2}\right). \tag{3.13}$$

Using the gaugino mass relation from eq. (3.6), lower bounds on the neutralino decay length $c\tau_{\chi_1^0}$ can then be derived from table 3 and figure 4. Our results are summarized in figure 10. For the parameter space allowed by EWPT and overproduction bounds, we obtain minimal decay lengths $\mathcal{O}(100\,{\rm m} - 10\,{\rm km})$, which are in the range of detectability of the LHC [37]. Decay lengths as small as $c\tau_{\chi_1^0} \simeq 50$ m are allowed for $m_{3/2} \simeq 17$ GeV et $m_{\chi_1^0} \simeq 110$ GeV.
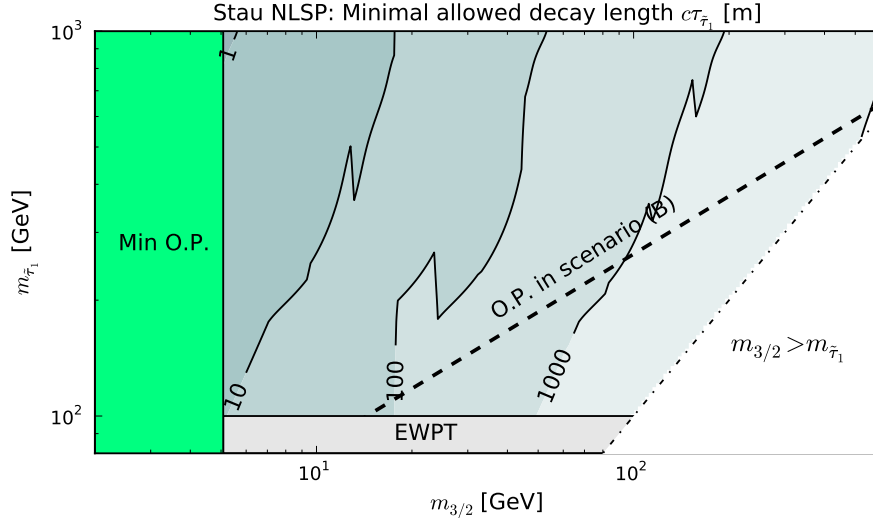
Figure 9. Contour plot of lower bounds on the stau NLSP decay length coming from the gamma-ray line constraints on the gravitino lifetime, as function of the stau and gravitino masses, $m_{\tilde{\tau}_1}$ and $m_{3/2}$ respectively. The lower gray region is excluded by electroweak precision tests (EWPT). For thermal leptogenesis, overproduction (O.P.) of gravitinos excludes at minimum the left green region, a limit which strengthens to the black-dashed line when assuming the universal boundary conditions (B), cf. eq. (3.5). The lower-right exclusion comes from the gravitino LSP requirement. Note that for high gravitino masses above a few hundred GeV our adopted line search strategy might overestimate the limits on the NLSP decay length, because the branching ratio into gamma-ray lines can become very small (see text).
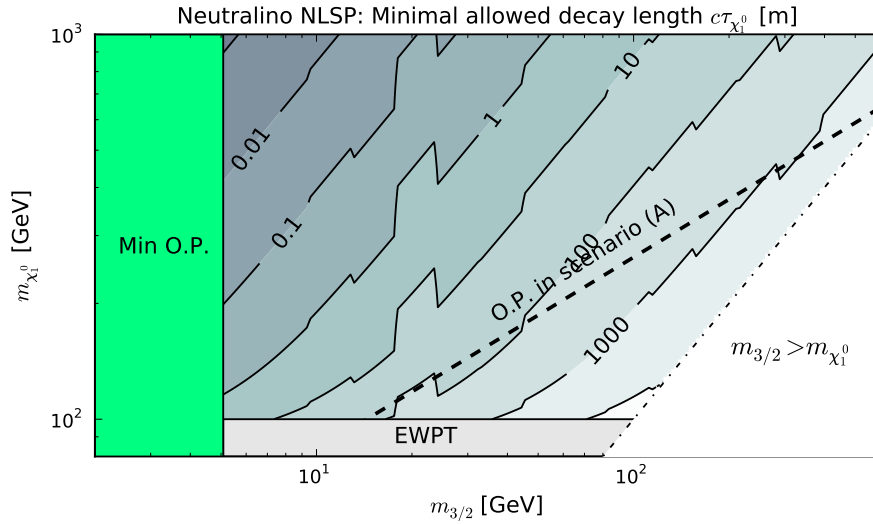

Figure 10. Like figure 9, but for a neutralino NLSP.

4 Conclusions

We have presented a dedicated search for gamma-ray lines with energies between 1 and 300 GeV in the diffuse gamma-ray fluxes measured by Fermi LAT between 4 Aug 2008 and 17 Nov 2010, based on the public 'DataClean' event class. Such lines could be produced

in dark matter annihilation or decay, and they are highly relevant for dark matter searches since they provide an essentially background free signature. To calculate the significance of potential gamma-ray lines in the diffuse flux, we used a binned profile likelihood method and fitted the observed energy spectrum locally with a line signal as expected from decaying or annihilating dark matter inside the Galactic halo plus a power law that resembles the astrophysical background fluxes. No gamma-ray lines were found at 5σ confidence level, and we derived conservative upper limits on the gamma-ray line flux that comes from regions with high Galactic latitudes or from the Galactic center (table 3). We also discussed the apparent presence of several line-like features at the few percent level in the public data, which appear at energies below $20\,\mathrm{GeV}$ with $\sim 3\sigma$ significance and which are most probably due to instrumental effects.

Our conservative upper limits on the partial annihilation cross section of WIMP dark matter into γ-pairs, $\langle\sigma v\rangle_{\psi\psi\to\gamma\gamma}$, improve the EGRET limits in the range $E_\gamma = 1\text{--}10\,\mathrm{GeV}$ by up to an order of magnitude, while the previous Fermi LAT results ($E_\gamma = 30\text{--}200\,\mathrm{GeV}$) are updated with two years of data and extended to the larger energy range $E_\gamma = 1\text{--}300\,\mathrm{GeV}$ (figure 5). Despite the increased statistics and the choice of a sky-region with optimized signal-to-noise ratio, the previous Fermi LAT limits are however only slightly improved. The reason is a somewhat worse energy resolution of the public data with respect to the dedicated Fermi LAT analysis as well as our strategy to always quote conservative limits in certain energy bands. The lower bounds on the inverse decay widths of dark matter into monochromatic photons, $\Gamma_{\psi\to\gamma\nu}^{-1}$, are at the level of $6 \times 10^{28}\,\mathrm{s}$ over most of the considered energy regime (figure 4). Our results also constrain annihilation and decay channels with γZ^0 final states.

In a R-parity breaking supersymmetric framework with gravitino LSP, we used the results of our gamma-ray line search to derive lower bounds on the gravitino lifetime. Considering supergravity models with two different types of universal boundary conditions at the grand unification scale, these lifetime constraints were used to set lower limits on the corresponding NLSP decay lengths. For gravitino and NLSP masses compatible with electroweak precision tests and overproduction constraints, we obtain $\mathcal{O}(100\,\mathrm{m} - 10\,\mathrm{km})$ lower bounds on the NLSPs decay lengths. Interestingly, all these decay lengths would be accessible at the LHC.

Note added. During the final stages of this work, first LHC limits on the CMSSM parameter space were published by the CMS collaboration [112], which will further constrain the superparticle masses discussed in this paper. Furthermore, the anonymous referee pointed us to a talk about the ongoing gamma-ray line analysis by the Fermi LAT collaboration, where preliminary results are presented that are, where they overlap, in agreement with our findings, and where line-like artefacts at lower energies in the current public data are mentioned.[15]

---

[15]See talk by E. Bloom at Aspen Winter Workshop on Indirect and Direct Detection of Dark Matter, Feb 2011, `http://www.slac.stanford.edu/exp/glast/aspen11/talks.asp`

References

[1] G. Jungman, M. Kamionkowski and K. Griest, *Supersymmetric dark matter*, *Phys. Rept.* **267** (1996) 195 [`hep-ph/9506380`] [SPIRES].

[2] L. Bergstrom, *Non-baryonic dark matter: observational evidence and detection methods*, *Rept. Prog. Phys.* **63** (2000) 793 [`hep-ph/0002126`] [SPIRES].

[3] G. Bertone, D. Hooper and J. Silk, *Particle dark matter: evidence, candidates and constraints*, *Phys. Rept.* **405** (2005) 279 [`hep-ph/0404175`] [SPIRES].

[4] M. Srednicki, S. Theisen and J. Silk, *Cosmic quarkonium: a probe of dark matter*, *Phys. Rev. Lett.* **56** (1986) 263 [SPIRES].

[5] S. Rudaz, *Cosmic production of quarkonium?*, *Phys. Rev. Lett.* **56** (1986) 2128 [SPIRES].

[6] L. Bergstrom and H. Snellman, *Observable monochromatic photons from cosmic photino annihilation*, *Phys. Rev.* **D 37** (1988) 3737 [SPIRES].

[7] S.P. Martin, *A supersymmetry primer*, `hep-ph/9709356` [SPIRES].

[8] S. Rudaz and F.W. Stecker, *On the observability of the gamma-ray line flux from dark matter annihilation*, *Astrophys. J.* **368** (1991) 406 [SPIRES].

[9] L. Bergstrom, P. Ullio and J.H. Buckley, *Observability of gamma rays from dark matter neutralino annihilations in the Milky Way halo*, *Astropart. Phys.* **9** (1998) 137 [`astro-ph/9712318`] [SPIRES].

[10] L. Bergstrom and P. Ullio, *Full one-loop calculation of neutralino annihilation into two photons*, *Nucl. Phys.* **B 504** (1997) 27 [`hep-ph/9706232`] [SPIRES].

[11] Z. Bern, P. Gondolo and M. Perelstein, *Neutralino annihilation into two photons*, *Phys. Lett.* **B 411** (1997) 86 [`hep-ph/9706538`] [SPIRES].

[12] P. Ullio and L. Bergstrom, *Neutralino annihilation into a photon and a Z boson*, *Phys. Rev.* **D 57** (1998) 1962 [`hep-ph/9707333`] [SPIRES].

[13] P. Scott et al., *Direct constraints on minimal supersymmetry from Fermi-LAT observations of the dwarf galaxy Segue 1*, *JCAP* **01** (2010) 031 [`arXiv:0909.3300`] [SPIRES].

[14] J. Ripken, J. Conrad and P. Scott, *Direct constraints on the CMSSM using H.E.S.S. observations of the galactic centre and the Sagittarius dwarf galaxy*, `arXiv:1012.3939` [SPIRES].

[15] S. Profumo, *Hunting the lightest lightest neutralinos*, *Phys. Rev.* **D 78** (2008) 023507 [`arXiv:0806.2150`] [SPIRES].

[16] F. Ferrer, L.M. Krauss and S. Profumo, *Indirect detection of light neutralino dark matter in the NMSSM*, *Phys. Rev.* **D 74** (2006) 115007 [`hep-ph/0609257`] [SPIRES].

[17] S. Profumo, L. Ubaldi and C. Wainwright, *Singlet scalar dark matter: monochromatic gamma rays and metastable vacua*, *Phys. Rev.* **D 82** (2010) 123514 [`arXiv:1009.5377`] [SPIRES].

[18] E. Dudas, Y. Mambrini, S. Pokorski and A. Romagnoni, *(In)visible Z' and dark matter*, *JHEP* **08** (2009) 014 [`arXiv:0904.1745`] [SPIRES].

[19] Y. Mambrini, *A clear dark matter gamma ray line generated by the Green-Schwarz mechanism*, *JCAP* **12** (2009) 005 [`arXiv:0907.2918`] [SPIRES].

[20] Y. Mambrini, *Specific dark matter signatures from hidden* U(1), `PoS(QFTHEP2010)027` [`arXiv:1012.0447`] [SPIRES].

[21] J. Goodman et al., *Gamma ray line constraints on effective theories of dark matter*, *Nucl. Phys.* **B 844** (2011) 55 [`arXiv:1009.0008`] [SPIRES].

[22] C.B. Jackson, G. Servant, G. Shaughnessy, T.M.P. Tait and M. Taoso, *Higgs in space!*, *JCAP* **04** (2010) 004 [arXiv:0912.0004] [SPIRES].

[23] M. Gustafsson, E. Lundstrom, L. Bergstrom and J. Edsjo, *Significant gamma lines from inert Higgs dark matter*, *Phys. Rev. Lett.* **99** (2007) 041301 [astro-ph/0703512] [SPIRES].

[24] G. Bertone, C.B. Jackson, G. Shaughnessy, T.M.P. Tait and A. Vallinotto, *The WIMP forest: indirect detection of a chiral square*, *Phys. Rev.* **D 80** (2009) 023512 [arXiv:0904.1442] [SPIRES].

[25] G. Bertone, C.B. Jackson, G. Shaughnessy, T.M.P. Tait and A. Vallinotto, *Gamma ray lines from a universal extra dimension*, arXiv:1009.5107 [SPIRES].

[26] L. Bergstrom, T. Bringmann, M. Eriksson and M. Gustafsson, *Gamma rays from heavy neutralino dark matter*, *Phys. Rev. Lett.* **95** (2005) 241301 [hep-ph/0507229] [SPIRES].

[27] A. Birkedal, K.T. Matchev, M. Perelstein and A. Spray, *Robust gamma ray signature of WIMP dark matter*, hep-ph/0507194 [SPIRES].

[28] T. Bringmann, L. Bergstrom and J. Edsjo, *New gamma-ray contributions to supersymmetric dark matter annihilation*, *JHEP* **01** (2008) 049 [arXiv:0710.3169] [SPIRES].

[29] L. Bergstrom, T. Bringmann, M. Eriksson and M. Gustafsson, *Gamma rays from Kaluza-Klein dark matter*, *Phys. Rev. Lett.* **94** (2005) 131301 [astro-ph/0410359] [SPIRES].

[30] W. Buchmüller, L. Covi, K. Hamaguchi, A. Ibarra and T. Yanagida, *Gravitino dark matter in R-parity breaking vacua*, *JHEP* **03** (2007) 037 [hep-ph/0702184] [SPIRES].

[31] F. Takayama and M. Yamaguchi, *Gravitino dark matter without R-parity*, *Phys. Lett.* **B 485** (2000) 388 [hep-ph/0005214] [SPIRES].

[32] G. Bertone, W. Buchmüller, L. Covi and A. Ibarra, *Gamma-rays from decaying dark matter*, *JCAP* **11** (2007) 003 [arXiv:0709.2299] [SPIRES].

[33] A. Ibarra and D. Tran, *Gamma ray spectrum from gravitino dark matter decay*, *Phys. Rev. Lett.* **100** (2008) 061301 [arXiv:0709.4593] [SPIRES].

[34] S. Lola, P. Osland and A.R. Raklev, *Radiative gravitino decays from R-parity violation*, *Phys. Lett.* **B 656** (2007) 83 [arXiv:0707.2510] [SPIRES].

[35] A. Ibarra and D. Tran, *Antimatter signatures of gravitino dark matter decay*, *JCAP* **07** (2008) 002 [arXiv:0804.4596] [SPIRES].

[36] K. Ishiwata, S. Matsumoto and T. Moroi, *High energy cosmic rays from the decay of gravitino dark matter*, *Phys. Rev.* **D 78** (2008) 063505 [arXiv:0805.1133] [SPIRES].

[37] K. Ishiwata, T. Ito and T. Moroi, *Long-lived unstable superparticles at the LHC*, *Phys. Lett.* **B 669** (2008) 28 [arXiv:0807.0975] [SPIRES].

[38] L. Covi, M. Grefe, A. Ibarra and D. Tran, *Unstable gravitino dark matter and neutrino flux*, *JCAP* **01** (2009) 029 [arXiv:0809.5030] [SPIRES].

[39] W. Buchmüller, A. Ibarra, T. Shindou, F. Takayama and D. Tran, *Probing gravitino dark matter*, *JCAP* **09** (2009) 021 [arXiv:0906.1187] [SPIRES].

[40] K.-Y. Choi, D.E. Lopez-Fogliani, C. Muñoz and R.R. de Austri, *Gamma-ray detection from gravitino dark matter decay in the $\mu\nu SSM$*, *JCAP* **03** (2010) 028 [arXiv:0906.3681] [SPIRES].

[41] N.E. Bomark, S. Lola, P. Osland and A.R. Raklev, *Photon, neutrino and charged particle spectra from R-violating gravitino decays*, *Phys. Lett.* **B 686** (2010) 152 [arXiv:0911.3376] [SPIRES].

[42] K.-Y. Choi and C.E. Yaguna, *New decay modes of gravitino dark matter*, *Phys. Rev.* **D 82** (2010) 015008 [arXiv:1003.3401] [SPIRES].

[43] K.-Y. Choi, D. Restrepo, C.E. Yaguna and O. Zapata, *Indirect detection of gravitino dark matter including its three-body decays*, *JCAP* **10** (2010) 033 [arXiv:1007.1728] [SPIRES].

[44] D. Eichler, *TeV particles as weakly unstable dark matter*, *Phys. Rev. Lett.* **63** (1989) 2440 [SPIRES].

[45] A. Arvanitaki et al., *Decaying dark matter as a probe of unification and TeV spectroscopy*, *Phys. Rev.* **D 80** (2009) 055011 [arXiv:0904.2789] [SPIRES].

[46] C. Arina, T. Hambye, A. Ibarra and C. Weniger, *Intense gamma-ray lines from hidden vector dark matter decay*, *JCAP* **03** (2010) 024 [arXiv:0912.4496] [SPIRES].

[47] PAMELA collaboration, O. Adriani et al., *An anomalous positron abundance in cosmic rays with energies 1.5–100 GeV*, *Nature* **458** (2009) 607 [arXiv:0810.4995] [SPIRES].

[48] THE FERMI LAT collaboration, A.A. Abdo et al., *Measurement of the cosmic ray e+ plus e- spectrum from 20 GeV to 1 TeV with the Fermi Large Area Telescope*, *Phys. Rev. Lett.* **102** (2009) 181101 [arXiv:0905.0025] [SPIRES].

[49] THE FERMI LAT collaboration, M. Ackermann et al., *Fermi LAT observations of cosmic-ray electrons from 7 GeV to 1 TeV*, *Phys. Rev.* **D 82** (2010) 092004 [arXiv:1008.3999] [SPIRES].

[50] M. Garny, A. Ibarra, D. Tran and C. Weniger, *Gamma-ray lines from radiative dark matter decay*, *JCAP* **01** (2011) 032 [arXiv:1011.3786] [SPIRES].

[51] THE FERMI LAT collaboration, W.B. Atwood et al., *The Large Area Telescope on the Fermi gamma-ray space telescope mission*, *Astrophys. J.* **697** (2009) 1071 [arXiv:0902.1089] [SPIRES].

[52] A.A. Abdo et al., *Fermi LAT search for photon lines from 30 to 200 GeV and dark matter implications*, *Phys. Rev. Lett.* **104** (2010) 091302 [arXiv:1001.4836] [SPIRES].

[53] A.R. Pullen, R.-R. Chary and M. Kamionkowski, *Search with EGRET for a gamma ray line from the galactic center*, *Phys. Rev.* **D 76** (2007) 063006 [astro-ph/0610295] [SPIRES].

[54] THE FERMI-LAT collaboration, A.A. Abdo et al., *The spectrum of the isotropic diffuse gamma-ray emission derived from first-year Fermi Large Area Telescope data*, *Phys. Rev. Lett.* **104** (2010) 101101 [arXiv:1002.3603] [SPIRES].

[55] THE FERMI-LAT collaboration, A.A. Abdo et al., *Constraints on cosmological dark matter annihilation from the Fermi-LAT isotropic diffuse gamma-ray measurement*, *JCAP* **04** (2010) 014 [arXiv:1002.4415] [SPIRES].

[56] L. Bergstrom, J. Edsjo and P. Ullio, *Spectral gamma-ray signatures of cosmological dark matter annihilations*, *Phys. Rev. Lett.* **87** (2001) 251301 [astro-ph/0105048] [SPIRES].

[57] P. Ullio, L. Bergstrom, J. Edsjo and C.G. Lacey, *Cosmological dark matter annihilations into gamma-rays: a closer look*, *Phys. Rev.* **D 66** (2002) 123502 [astro-ph/0207125] [SPIRES].

[58] G.D. Mack, T.D. Jacques, J.F. Beacom, N.F. Bell and H. Yuksel, *Conservative constraints on dark matter annihilation into gamma rays*, *Phys. Rev.* **D 78** (2008) 063542 [arXiv:0803.0157] [SPIRES].

[59] H. Yuksel and M.D. Kistler, *Circumscribing late dark matter decays model-independently*, *Phys. Rev.* **D 78** (2008) 023502 [arXiv:0711.2906] [SPIRES].

[60] P.D. Serpico and G. Zaharijas, *Optimal angular window for observing dark matter annihilation from the galactic center region: the case of gamma-ray lines*, *Astropart. Phys.* **29** (2008) 380 [arXiv:0802.3245] [SPIRES].

[61] P.D. Serpico and D. Hooper, *Gamma rays from dark matter annihilation in the central region of the galaxy*, *New J. Phys.* **11** (2009) 105010 [arXiv:0902.2539] [SPIRES].

[62] Z.-C. Tang, Q. Yuan, X.-J. Bi and G.-M. Chen, *On the detectability of galactic dark matter annihilation into monochromatic gamma-rays*, arXiv:1008.2046 [SPIRES].

[63] THE CDMS-II collaboration, Z. Ahmed et al., *Dark matter search results from the CDMS II experiment*, *Science* **327** (2010) 1619 [arXiv:0912.3592] [SPIRES].

[64] CoGeNT collaboration, C.E. Aalseth et al., *Results from a search for light-mass dark matter with a P-type point contact germanium detector*, *Phys. Rev. Lett.* **106** (2011) 131301 [arXiv:1002.4703] [SPIRES].

[65] DAMA collaboration, R. Bernabei et al., *First results from DAMA/LIBRA and the combined results with DAMA/NaI*, *Eur. Phys. J.* **C 56** (2008) 333 [arXiv:0804.2741] [SPIRES].

[66] R. Bernabei et al., *New results from DAMA/LIBRA*, *Eur. Phys. J.* **C 67** (2010) 39 [arXiv:1002.1028] [SPIRES].

[67] A.M. Ghez et al., *Measuring distance and properties of the Milky Way's central supermassive black hole with stellar orbits*, *Astrophys. J.* **689** (2008) 1044 [arXiv:0808.2870] [SPIRES].

[68] S. Gillessen et al., *Monitoring stellar orbits around the massive black hole in the galactic center*, *Astrophys. J.* **692** (2009) 1075 [arXiv:0810.4674] [SPIRES].

[69] J.F. Navarro, C.S. Frenk and S.D.M. White, *A universal density profile from hierarchical clustering*, *Astrophys. J.* **490** (1997) 493 [astro-ph/9611107] [SPIRES].

[70] J.F. Navarro et al., *The inner structure of LambdaCDM halos III: universality and asymptotic slopes*, *Mon. Not. Roy. Astron. Soc.* **349** (2004) 1039 [astro-ph/0311231] [SPIRES].

[71] V. Springel et al., *The Aquarius project: the subhalos of galactic halos*, *Mon. Not. Roy. Astron. Soc.* **391** (2008) 1685 [arXiv:0809.0898] [SPIRES].

[72] L. Pieri, J. Lavalle, G. Bertone and E. Branchini, *Implications of high-resolution simulations on indirect dark matter searches*, *Phys. Rev.* **D 83** (2011) 023518 [arXiv:0908.0195] [SPIRES].

[73] P. Salucci et al., *The universal rotation curve of spiral galaxies. II: The dark matter distribution out to the virial radius*, *Mon. Not. Roy. Astron. Soc.* **378** (2007) 41 [astro-ph/0703115] [SPIRES].

[74] P. Salucci, F. Nesti, G. Gentile and C.F. Martins, *The dark matter density at the Sun's location*, *Astron. Astrophys.* **523** (2010) A83 [arXiv:1003.3101] [SPIRES].

[75] R. Catena and P. Ullio, *A novel determination of the local dark matter density*, *JCAP* **08** (2010) 004 [arXiv:0907.0018] [SPIRES].

[76] GLAST LAT collaboration, Y. Edmonds et al., *Estimate for GLAST LAT Milky Way dark matter WIMP line sensitivity*, *AIP Conf. Proc.* **921** (2007) 514 [SPIRES].

[77] http://fermi.gsfc.nasa.gov/ssc/data/analysis/LAT_caveats.html.

[78] THE FERMI LAT collaboration, R. Rando, *Post-launch performance of the Fermi Large Area Telescope*, arXiv:0907.0626 [SPIRES].

[79] THE FERMI LAT collaboration, A.A. Abdo et al., *The on-orbit calibrations for the Fermi Large Area Telescope*, *Astropart. Phys.* **32** (2009) 193 [arXiv:0904.2226] [SPIRES].

[80] W.A. Rolke, A.M. Lopez and J. Conrad, *Limits and confidence intervals in the presence of nuisance parameters*, *Nucl. Instrum. Meth.* **A 551** (2005) 493 [physics/0403059] [SPIRES].

[81] J. Conrad, T. Ylinen and J. Scargle, *Statistical analysis of detection of, and upper limits on, dark matter lines*, *AIP Conf. Proc.* **921** (2007) 586 [SPIRES].

[82] S.S. Wilks, *The large-sample distribution of the likelihood ratio for testing composite hypotheses*, *Ann. Math. Statist.* **9** (1938) 60.

[83] G.J. Feldman and R.D. Cousins, *A unified approach to the classical statistical analysis of small signals*, *Phys. Rev.* **D 57** (1998) 3873 [physics/9711021] [SPIRES].

[84] THE FERMI LAT collaboration, T. Ylinen, *Annihilation lines from dark matter with the Fermi-LAT*, *AIP Conf. Proc.* **1241** (2010) 463 [SPIRES].

[85] H. Pagels and J.R. Primack, *Supersymmetry, cosmology and new TeV physics*, *Phys. Rev. Lett.* **48** (1982) 223 [SPIRES].

[86] M. Bolz, A. Brandenburg and W. Buchmüller, *Thermal production of gravitinos*, *Nucl. Phys.* **B 606** (2001) 518 [hep-ph/0012052] [SPIRES].

[87] J. Pradler and F.D. Steffen, *Thermal gravitino production and collider tests of leptogenesis*, *Phys. Rev.* **D 75** (2007) 023509 [hep-ph/0608344] [SPIRES].

[88] W. Buchmüller, M. Endo and T. Shindou, *Superparticle mass window from leptogenesis and decaying gravitino dark matter*, *JHEP* **11** (2008) 079 [arXiv:0809.4667] [SPIRES].

[89] WMAP collaboration, E. Komatsu et al., *Seven-year Wilkinson Microwave Anisotropy Probe (WMAP) observations: cosmological interpretation*, *Astrophys. J. Suppl.* **192** (2011) 18 [arXiv:1001.4538] [SPIRES].

[90] M. Fukugita and T. Yanagida, *Baryogenesis without grand unification*, *Phys. Lett.* **B 174** (1986) 45 [SPIRES].

[91] W. Buchmüller, P. Di Bari and M. Plümacher, *Leptogenesis for pedestrians*, *Ann. Phys.* **315** (2005) 305 [hep-ph/0401240] [SPIRES].

[92] J.R. Ellis, D.V. Nanopoulos and S. Sarkar, *The cosmology of decaying gravitinos*, *Nucl. Phys.* **B 259** (1985) 175 [SPIRES].

[93] S. Sarkar, *Big bang nucleosynthesis and physics beyond the standard model*, *Rept. Prog. Phys.* **59** (1996) 1493 [hep-ph/9602260] [SPIRES].

[94] M. Kawasaki, K. Kohri and T. Moroi, *Big-bang nucleosynthesis and hadronic decay of long-lived massive particles*, *Phys. Rev.* **D 71** (2005) 083502 [astro-ph/0408426] [SPIRES].

[95] M. Pospelov, *Particle physics catalysis of thermal big bang nucleosynthesis*, *Phys. Rev. Lett.* **98** (2007) 231301 [hep-ph/0605215] [SPIRES].

[96] K. Hamaguchi, T. Hatsuda, M. Kamimura, Y. Kino and T.T. Yanagida, *Stau-catalyzed Li-6 production in big-bang nucleosynthesis*, *Phys. Lett.* **B 650** (2007) 268 [hep-ph/0702274] [SPIRES].

[97] M. Pospelov, J. Pradler and F.D. Steffen, *Constraints on supersymmetric models from catalytic primordial nucleosynthesis of beryllium*, *JCAP* **11** (2008) 020 [arXiv:0807.4287] [SPIRES].

[98] M. Kawasaki, K. Kohri, T. Moroi and A. Yotsuyanagi, *Big-bang nucleosynthesis and gravitino*, *Phys. Rev.* **D 78** (2008) 065011 [arXiv:0804.3745] [SPIRES].

[99] T. Kanzaki, M. Kawasaki, K. Kohri and T. Moroi, *Cosmological constraints on gravitino LSP scenario with sneutrino NLSP*, *Phys. Rev.* **D 75** (2007) 025011 [hep-ph/0609246] [SPIRES].

[100] J.L. Diaz-Cruz, J.R. Ellis, K.A. Olive and Y. Santoso, *On the feasibility of a stop NLSP in gravitino dark matter scenarios*, *JHEP* **05** (2007) 003 [hep-ph/0701229] [SPIRES].

[101] J. Pradler and F.D. Steffen, *Constraints on the reheating temperature in gravitino dark matter scenarios*, *Phys. Lett.* **B 648** (2007) 224 [hep-ph/0612291] [SPIRES].

[102] A. De Simone, M. Garny, A. Ibarra and C. Weniger, *Supersymmetric leptogenesis with a light hidden sector*, *JCAP* **07** (2010) 017 [arXiv:1004.4890] [SPIRES].

[103] C. Cheung, J. Mardon, Y. Nomura and J. Thaler, *A definitive signal of multiple supersymmetry breaking*, *JHEP* **07** (2010) 035 [arXiv:1004.4637] [SPIRES].

[104] W. Buchmüller, K. Schmitz and G. Vertongen, *Matter and dark matter from false vacuum decay*, *Phys. Lett.* **B 693** (2010) 421 [arXiv:1008.2355] [SPIRES].

[105] W. Buchmüller, K. Schmitz and G. Vertongen, *Entropy, baryon asymmetry and dark matter from heavy neutrino decays*, [`arXiv:1104.2750`] [SPIRES].

[106] J. Schmidt, C. Weniger and T.T. Yanagida, *Dynamical matter-parity breaking and gravitino dark matter*, *Phys. Rev.* **D 82** (2010) 103517 [`arXiv:1008.0398`] [SPIRES].

[107] S. Bobrovskyi, W. Buchmüller, J. Hajer and J. Schmidt, *Broken R-parity in the sky and at the LHC*, *JHEP* **10** (2010) 061 [`arXiv:1007.5007`] [SPIRES].

[108] PARTICLE DATA GROUP collaboration, K. Nakamura et al., *Review of particle physics*, *J. Phys.* **G 37** (2010) 075021 [SPIRES].

[109] J. Alwall, M.-P. Le, M. Lisanti and J.G. Wacker, *Searching for directly decaying gluinos at the Tevatron*, *Phys. Lett.* **B 666** (2008) 34 [`arXiv:0803.0019`] [SPIRES].

[110] B. Mukhopadhyaya, S. Roy and F. Vissani, *Correlation between neutrino oscillations and collider signals of supersymmetry in an R-parity violating model*, *Phys. Lett.* **B 443** (1998) 191 [`hep-ph/9808265`] [SPIRES].

[111] E.J. Chun and J.S. Lee, *Implication of super-Kamiokande data on R-parity violation*, *Phys. Rev.* **D 60** (1999) 075006 [`hep-ph/9811201`] [SPIRES].

[112] CMS collaboration, V. Khachatryan et al., *Search for supersymmetry in pp collisions at 7 TeV in events with jets and missing transverse energy*, *Phys. Lett.* **B 698** (2011) 196 [`arXiv:1101.1628`] [SPIRES].